

Proceedings Article

Safe and Rapid 3D Imaging: Upgrade of a Human-Sized Brain MPI System

Florian Thieben ^{a,b,*}, Fabian Mohn ^{a,b}, Fynn Foerger ^{a,b}, Niklas Hackelberg ^{a,b},
Jan-Philipp Scheel ^{c,d}, Matthias Graeser ^{a,b,c,d}, Tobias Knopp ^{a,b}

^aSection for Biomedical Imaging, University Medical Center Hamburg-Eppendorf, Hamburg, Germany

^bInstitute for Biomedical Imaging, Hamburg University of Technology, Hamburg, Germany

^cFraunhofer Research Institute for Individualized and Cell-based Medicine, Lübeck, Germany

^dInstitute for Medical Engineering, University of Lübeck, Lübeck, Germany

*Corresponding author, email: f.thieben@uke.de

© 2023 Thieben *et al.*; licensee Infinite Science Publishing GmbH

This is an Open Access article distributed under the terms of the Creative Commons Attribution License (<http://creativecommons.org/licenses/by/4.0>), which permits unrestricted use, distribution, and reproduction in any medium, provided the original work is properly cited.

Abstract

Magnetic Particle Imaging hardware has reached human scale and thus patient safety questions and clinical application scenarios are in the focus of current research. In this work, we present a safe real-time 3D MPI system for cerebral applications. High voltages are avoided to ensure patient safety by a low voltage-high current transmit coil design. The developed 2D drive-field generator generates a field-free-point trajectory in the sagittal xz -plane that is shifted with low frequency by a dynamic selection-field sequence along the y -axis. The scanner generates 3D images with 4 frames/second and allows for direct visualization of the clinically preferred transversal yz -plane, which is crucial for future brain examinations. Advanced reconstruction techniques reach a system sensitivity of $4 \mu\text{g}_{\text{Fe}}$ with respect to the iron mass in a sensitivity study.

1. Introduction

Preclinical animal studies have shown the potential of Magnetic Particle Imaging (MPI) in the direction of stroke detection, cancer tracking, and angiography [1]. Currently, MPI hardware development is moving towards human studies [2–4]. In [4], Graeser et al. presented a prototype of a 2D human-sized MPI device for brain applications and showcased the capabilities of the system in static and dynamic phantom studies. A robot shifted selection-field generator (SFG) was used to move the dynamic selection field in z -direction enabling slice selection. The prototype was only capable of rapid imaging in the coronal xy -plane, which is sub-optimal for clinical practice where commonly transversal yz -slices are considered for examinations of the brain [5].

For first human trials, various safety aspects must

be regarded, which already need to be accounted for in the hard- and software design phase. In particular, the applied oscillating magnetic drive fields need to stay below amplitudes that may cause any peripheral nerve stimulation (PNS) at the human head. While pre-clinical MPI can safely operate with drive-field amplitudes up to 20 mT [1], Ozaslan et al. have shown in [6] that PNS limits the maximum drive-field amplitude for human brain experiments to about 3 to 5 mT. Besides PNS, electrical safety against burns or discharges must be guaranteed. To prevent any voltage breakdown, the large voltage drop across the drive-field generator (DFG) coils can be minimized by litz-wire parallelization in Rutherford configuration [7]. Consequently, the self-inductance is reduced and a higher current flowing in the coils is required to provide the same current density in the DFG. Furthermore, the concept of an inductive coupling network (ICN) can

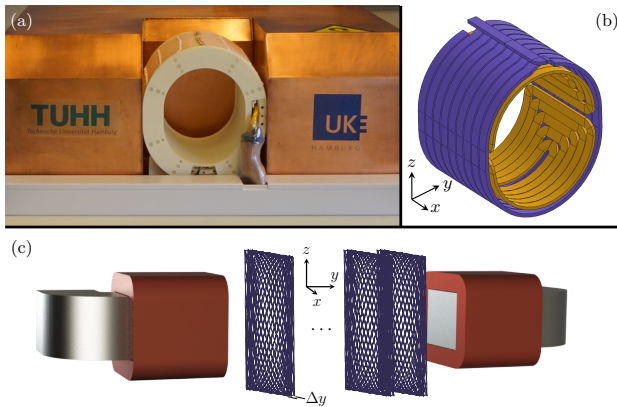


Figure 1: Headscanner. Picture of human head sized MPI system (main axes of the bore ellipse: 21.6 cm, 17.5 cm) (a). The two-dimensional excitation coil consists of a solenoid in x -direction (purple) and a saddle coil in z -direction (yellow) (b). The 2D drive-field FOV spanned in the xz plane is moved in y -direction by a dynamic selection field generated by a Maxwell coil pair with iron cores (c).

be used to gain a differential and floating potential instead of high potentials towards ground in proximity to the human head [8].

These safety design considerations motivate the following upgrade to the first generation of the human head scanner developed in [4]: First, a new 2D DFG with excitation in xz -direction, enabling fully 3D real-time imaging without mechanical components. Second, a system that has low voltages and galvanically separated transmission- and receive-coil circuits (floating potential) at the target drive-field strength of 5 mT. This short paper gives an overview of the key design aspects of the hardware and shows first 3D imaging results.

II. Methods and materials

Setup: The 3D MPI system in Figure 1(a) is located in an unshielded environment and the DFG consists of two orthogonal drive-field coils in x - and z -directions (Figure 1 (b)) and is enclosed by a proper polyamid insulation (Figure 2 (a)). A Rutherford-wire configuration with 12 parallel litz-wire cables is used in combination with low-power-loss ICNs to reach high currents at low voltages. A 2D Lissajous trajectory in the xz -plane is created by a 5 mT excitation at 25.699 kHz in the x -coil and a 4 mT excitation at 26.042 kHz in the z -coil. The channels are orthogonal and decoupled by a capacitor reaching -35 dB cross-coupling.

The SFG of [4] is used to generate a 0.21 T/m gradient in y -direction. Using a dynamic selection-field sequence, the SFG moves the field-free-point (FFP) along the y -axis (Figure 1 (c)). The combination of DFG and SFG reaches a temporal resolution of 4 frames/second.

For signal reception, a gradiometric receive coil in x -direction and a saddle coil in y -direction are used. The coils are connected to a differential 4th order band-stop filter, followed by a custom low-noise amplifier. The signal generation and digitization of the system is based on a cluster of RedPitaya STEMLab 125-14 hardware (Red Pitaya, Solkan, Slovenia) and our open-source software RedPitayaDAQServer [9]. The RedPitayas and other devices of the system are controlled by our open-source Julia framework *MPIMeasurements.jl* [10] to perform the imaging sequences in different measurement scenarios.

Experiments: To assess the sensitivity of the MPI system, a dilution series was prepared and measured. For this purpose, 50 μL samples with the tracer perimag (micro-mod Partikeltechnologie, Rostock, Germany) were filled with varying iron masses between 4 μg_{Fe} and 512 μg_{Fe} . Each sample was measured at three different positions within the field-of-view (FOV). The positions were oriented along a diagonal line crossing the FOV, spaced 35 mm apart with the middle position in the center. Prior to the measurements, a cubic 250 μL δ -sample filled with 17 $\mu\text{g}_{\text{Fe}}/\mu\text{L}$ (303.57 $\text{mmol}_{\text{Fe}}/\text{L}$) perimag was used to measure a system matrix on a $80 \times 80 \times 80 \text{ mm}^3$ FOV, with a grid size of $13 \times 13 \times 13$. To showcase the 3D imaging capability of the system, two opposing, nested U-shaped tubes with 3 mm inner diameter were filled with perimag containing 0.25 $\mu\text{g}_{\text{Fe}}/\mu\text{L}$ (4.47 $\text{mmol}_{\text{Fe}}/\text{L}$). The first was placed in the xy -plane with a length of 16 cm and an opening of 40 mm. The second was placed orthogonal in the xz -plane with a length of 14 cm and an opening of 45 mm. The corresponding system matrix was recorded with the aforementioned δ -sample on a $110 \times 110 \times 80 \text{ mm}^3$ FOV, with a grid size of $13 \times 13 \times 13$. **Reconstruction:** An advanced iterative Kaczmarz solver with an ℓ^1 sparsity constraint from the open-source Julia package *MPiReco.jl*¹ was used for image reconstruction. Frequency selection was done by omitting frequencies with low signal-to-noise ratio (SNR). For the different iron masses in the sensitivity study, the SNR-threshold, the iterations and the ℓ^1 and ℓ^2 regularization parameters λ_1 and λ_2 were adapted individually to match best image quality. To improve the visual aspects of the 3D-tube phantom, the corresponding system matrix was interpolated to a grid size of $19 \times 19 \times 13$ prior to the reconstruction.

III. Results

The Rutherford-wire configuration reduces the maximum coil voltage down to 535 V (240 A at 5 mT, 14.4 μH) and 480 V (301 A at 4 mT, 9.74 μH) for the x - and the z -coil, respectively. The typical dielectric breakdown strength of polyamid insulation is about 20 kV/mm [11]. Assuming an insulation thickness of at least 1 mm,

¹<https://github.com/MagneticParticleImaging/MPiReco.jl>

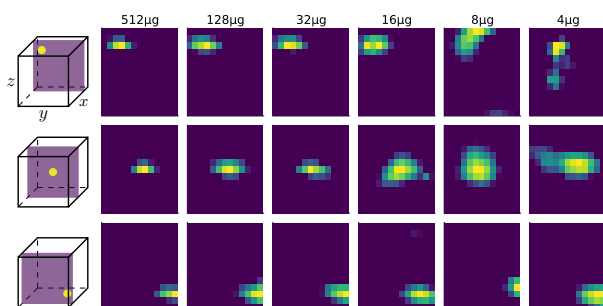


Figure 2: Concentration series. Reconstruction results in the transversal plane for different concentrations at three positions. The schematic cubes on the left symbolizes the FOV and show the imaging plane (purple). The sample position within the plan is marked by a dot (yellow).

Rutherford wire parallelization results in sufficient system safety margin by a factor of more than ~ 30 . Due to its transformation step, the ICN offers floating potentials in proximity to the human head and provides a high current-gain with low losses.

Floating potentials increase patient safety: Although the DFG is properly insulated, a possible failure scenario would be the exposure of an electrical connection and that the patient gets in contact with it. However, with floating potentials of the DFG and all its components, patient safety is increased, because the patient could only be injured if direct galvanic contact is made at two separate points simultaneously.

Figure 2 shows a series of reconstructions in the transversal yz -plane for different concentrations at three spatial positions. Down to an iron mass of 4 to 8 μg_{Fe} the positions could clearly be resolved for all three positions, although structural artifacts appear in the lowest two concentration steps. In Figure 3, the reconstruction of the U-shaped 3D tube phantom is shown with sagittal (a), transversal (b), and coronal (c) slices. In (d), a picture of the phantom is depicted, along with references for scale and orientation. The phantom is clearly resolved and features sharp edges, although x - and y -directions indicate superior resolution than in z -direction.

IV. Discussion and conclusion

In this work we presented a 3D imaging device with a large FOV ($110 \times 110 \times 80 \text{ mm}^3$) and high temporal resolution of 4 frames/second. The redesign of the transmit circuit can be considered safe for human experiments, in terms of electrical safety and PNS. The specific absorption rate limit of 4 W kg^{-1} is reached at 12 mT for 26 kHz, which is higher than the limit imposed by the peripheral nerve stimulation [12].

Regarding sensitivity, the reconstructed images of the $4 \mu\text{g}_{\text{Fe}}$ sample have several artifacts, but the diagonal spa-

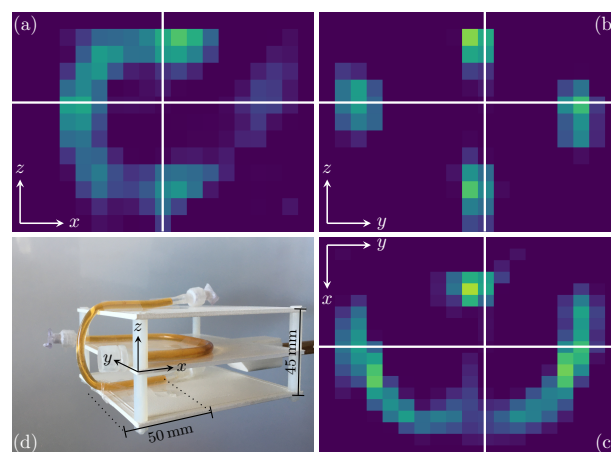


Figure 3: 3D Reconstructions. Three imaging planes of a tube phantom sagittal (a), transversal (b) and coronal (c) and the 3D tube phantom (d) are shown.

tial movement from one corner to the other is still visible. The experiments show high sensitivity over the entire FOV. 3D imaging experiments demonstrate volumetric reconstructions, including the preferred transversal yz -plane. The lower resolution in z -direction results from the lack of a dedicated z -receive coil. In this direction, the feed-through coupling is high due to the saddle-coil design and their narrow and inhomogeneous field profiles making it challenging to develop an efficient gradiometric receive coil. The concentration series and the reconstructed U-shaped 3D phantom already promise a sufficient sensitivity and resolution for similar perfusion experiments as performed in [4]. In conclusion, the presented system is now ready for human trials.

Acknowledgments

The authors thankfully acknowledge the financial support by the German Research Foundation (DFG, grant number KN 1108/7-1 and GR 5287/2-1).

Author's statement

Conflict of interest: Authors state no conflict of interest.

References

- [1] P. Ludewig, M. Graeser, N. D. Forkert, F. Thieben, J. Rández-Garbayo, J. Rieckhoff, K. Lessmann, F. Förger, P. Szargulski, T. Magnus, *et al.* Magnetic particle imaging for assessment of cerebral perfusion and ischemia. *Wiley Interdisciplinary Reviews: Nanomedicine and Nanobiotechnology*, 14(1):e1757, 2022.
- [2] P. Vogel, M. A. Rückert, C. Greiner, T. Reichl, J. Günther, A. von Boehn, L. Mirzozan, T. Kampf, T. A. Bley, S. Herz, *et al.* Impi-interventional magnetic particle imaging. *International Journal on Magnetic Particle Imaging*, 8(1 Suppl 1), 2022.

- [3] E. Mattingly, E. Mason, M. Sliwiak, and L. L. Wald. Drive and receive coil design for a human-scale mpi system. *International Journal on Magnetic Particle Imaging*, 8(1 Suppl 1), 2022.
- [4] M. Gräser, F. Thieben, P. Szwarzgulski, F. Werner, N. Gdaniec, M. Boberg, F. Griese, M. Möddel, P. Ludewig, D. van de Ven, *et al.* Human-sized magnetic particle imaging for brain applications. *Nature communications*, 10(1):1–9, 2019.
- [5] P. Ludewig, N. Gdaniec, J. Sedlacik, N. D. Forkert, P. Szwarzgulski, M. Graeser, G. Adam, M. G. Kaul, K. M. Krishnan, R. M. Ferguson, *et al.* Magnetic particle imaging for real-time perfusion imaging in acute stroke. *ACS nano*, 11(10):10480–10488, 2017.
- [6] A. A. Ozaslan, M. Utkur, U. Canpolat, M. A. Tuncer, K. K. Oguz, and E. U. Saritas. Pns limits for human head-size mpi systems: Preliminary results. *International Journal on Magnetic Particle Imaging*, 8(1 Suppl 1), 2022.
- [7] A. A. Ozaslan, A. R. Cagil, M. Graeser, T. Knopp, and E. U. Saritas. Design of a magnetostimulation head coil with rutherford cable winding. *International Journal on Magnetic Particle Imaging*, 6(2 Suppl 1), 2020.
- [8] T. F. Sattel, O. Woywode, J. Weizenecker, J. Rahmer, B. Gleich, and J. Borgert. Setup and validation of an mpi signal chain for a drive field frequency of 150 khz. *IEEE Transactions on Magnetics*, 51(2):1–3, 2015.
- [9] N. Hackelberg, J. Schumacher, M. Graeser, and T. Knopp. A flexible high-performance signal generation and digitization platform based on low-cost hardware. *International Journal on Magnetic Particle Imaging*, 8(1 Suppl 1), 2022.
- [10] N. Hackelberg, J. Schumacher, J. Ackers, M. Möddel, F. Foerger, M. Graeser, and T. Knopp. MPIMeasurements.jl: An Extensible Julia Framework for Composable Magnetic Particle Imaging Devices. *International Journal on Magnetic Particle Imaging*, 9(1 Suppl 1), 2023.
- [11] D. Kalaš, K. Šima, P. Kadlec, R. Polanský, R. Soukup, J. Řeboun, and A. Hamáček. Fff 3d printing in electronic applications: Dielectric and thermal properties of selected polymers. *Polymers*, 13(21):3702, 2021.
- [12] P. Chandrasekharan, Z. W. Tay, D. Hensley, X. Y. Zhou, B. K. Fung, C. Colson, Y. Lu, B. D. Fellows, Q. Huynh, C. Saayujya, *et al.* Using magnetic particle imaging systems to localize and guide magnetic hyperthermia treatment: Tracers, hardware, and future medical applications. *Theranostics*, 10(7):2965, 2020.